

Oxygen isotope variability in snow from western Dronning Maud Land, Antarctica and its relation to temperature

By M. M. HELSEN^{1*}, R. S. W. VAN DE WAL¹, M. R. VAN DEN BROEKE,¹ D. VAN AS¹,
H. A. J. MEIJER² and C. H. REIJMER¹, ¹*Institute for Marine and Atmospheric research Utrecht (IMAU),
PO Box 80.005, 3508 TA Utrecht, The Netherlands* ²*Centre for Isotope Research (CIO), Nijenborgh 4, 9747 AG
Groningen, The Netherlands*

(Manuscript received 23 December 2004; in final form 7 June 2005)

ABSTRACT

This paper presents $\delta^{18}\text{O}$ records from snow pits from four locations in Dronning Maud Land, Antarctica that contain at least four annual cycles. The aim of the study was to analyse in detail these records as well as the prevailing temperatures during accumulation in order to infer to what extent isotopic composition in this area can be interpreted as temperature information. The original seasonal amplitudes of the isotope records were reconstructed by use of a simple back-diffusion model. Automatic weather station data were used to describe the accumulation history and the near-surface temperatures; the temperatures at the atmospheric level of snow formation were inferred from a regional climate model. The results show that the strongly intermittent nature of the accumulation in this area can result in the exclusion of entire seasons from the isotope records. The temperature records also reveal that the oxygen isotope records in these snow pits are biased towards higher temperatures, since snowfall conditions are associated with higher temperatures. This effect is greatest at low temperatures. A comparison between the seasonal extreme isotopic and temperature values points out that on timescales of seasons to several years, isotopic variability cannot be interpreted with confidence as temperature changes at the accumulation sites.

1. Introduction

For decades the isotopic composition in polar snow has been regarded as a valuable temperature proxy and used as such in, for example, the Vostok ice core (Petit et al., 1999), the Greenland Ice Core Project (GRIP Members, 1993) and the recently obtained ice core from Dome C by the European Project for Ice Coring in Antarctica (EPICA Community Members, 2004). The basis of the use of oxygen isotopes in ice cores as a palaeothermometer is the strong spatial relationship between average local temperature (T) and the isotope composition of local precipitation at high and mid latitudes. The isotopic composition is usually expressed in ‰ as the deviation of a sample from the Vienna Standard Mean Ocean Water (V-SMOW) standard:

$$\delta^{18}\text{O} = \left[\frac{(^{18}\text{O}/^{16}\text{O})_{\text{sample}}}{(^{18}\text{O}/^{16}\text{O})_{\text{V-SMOW}}} \right] - 1.$$

The spatial $\delta^{18}\text{O}$ – T relationship (the so-called spatial slope) was first synthesized by Dansgaard (1964) and has often been used to interpret changes in $\delta^{18}\text{O}$ in ice cores in terms of temperature

changes. However, the use of the spatial slope might not always be justified in the interpretation of isotopic changes with time (Cuffey et al., 1995; Johnsen et al., 1995). Numerous other factors influence the $\delta^{18}\text{O}$ – T relationship, such as changing conditions in the water vapour source area (Merlivat and Jouzel, 1979), microphysical processes in clouds during snow formation (Fisher, 1991), changes in magnitude of the ratio between advective and diffusive transport (Kavanaugh and Cuffey, 2003), changes in the strength of the inversion layer (Van Lipzig et al., 2002) and seasonality in precipitation (Werner et al., 2000). Another phenomenon that can possibly influence the $\delta^{18}\text{O}$ – T relationship is the strong short-term relationship between precipitation and temperature: precipitation events in the polar region are often accompanied by higher temperatures than average (e.g. Loewe, 1936; Robin, 1983; Peel et al., 1988; Noone et al., 1999).

For central Antarctica, Jouzel et al. (2003) argued that the present-day spatial slope can serve as a surrogate for the temporal slope on glacial–interglacial timescales. On shorter timescales, however, the present-day spatial slope might not be equal to the temporal slope. Nevertheless, in some regions it appears possible to infer climate changes from isotope records in ice cores, at

*Corresponding author.
e-mail: m.m.helsen@phys.uu.nl

least on timescales of several decades (e.g. Arastarain et al., 1986; Masson-Delmotte et al., 2003). For short timescales, it may be possible to calibrate the $\delta^{18}\text{O}$ - T relationship with the seasonal temperature cycle (Shuman et al., 1995; Van Ommen and Morgan, 1997).

Within the framework of EPICA, a deep ice core is being drilled at Kohnen Station, Dronning Maud Land, Antarctica (DML; 75°S, 0°W), which is expected to provide a high-resolution climate record that covers more than a complete glacial cycle. To support the interpretation of the oxygen isotope signal from this core, numerous mass balance studies have been carried out with shallow and medium-length firn cores from DML (Isaksson et al., 1999; Oerter et al., 1999; Karlöf et al., 2000). Atmospheric modelling experiments have also been performed (Van Lipzig et al., 2002; Van den Broeke et al., 2002). Reijmer and Van den Broeke (2003) studied the mass balance of this area using automatic weather stations (AWSs). Their study shows that the interannual variability of precipitation is large in DML and that this potentially has a large effect on the oxygen isotope signal in this area.

Although comparisons of isotopic snow composition with the climate of DML are available (e.g. Oerter et al., 1999; Graf et al., 2002), direct comparisons between the observed isotopic composition of snow and prevailing meteorological conditions during snowfall events are sparse. McMorrow et al. (2001) carried out a detailed comparison between AWS data and isotope records for a different region in Antarctica, Law Dome, which is a high-accumulation area. Helsen et al. (in press) combined meteorological data with isotopic modelling to describe the depletion of the $\delta^{18}\text{O}$ value of the moisture over DML for one accumulation event. The present study aims to contribute to this topic by combining isotope records with meteorological observations from AWSs and to infer to what extent isotopic variability represents prevailing temperatures, with a focus on seasonal variability. Although the deep ice core at Kohnen Station is not expected to show a clear seasonal cycle (due to the low accumulation), the interpretation of isotope records from this ice core can benefit from knowledge of the nature of the local accumulation history.

Section 2 presents isotope records from shallow snow pits from four locations in western DML (Fig. 1). These snow pits were sampled in the vicinity of the AWSs in the field season 2001–2002; the isotope records cover the operational period of the AWSs (1998–2001). To correct for the influence of post-depositional diffusion in the snow pits, the original seasonal isotopic extremes must be reconstructed. This can be done with a simple back-diffusion model, as described in Section 3. Section 4 contains the accumulation history, derived from data from sonic height rangiers (SHRs), which monitor (the change in) surface height in the vicinity of the sampling locations (Reijmer and Van den Broeke, 2003). With the temperature and accumulation data from the AWSs, we constructed profiles of condensation temperature for the snow as a function of current depth. These

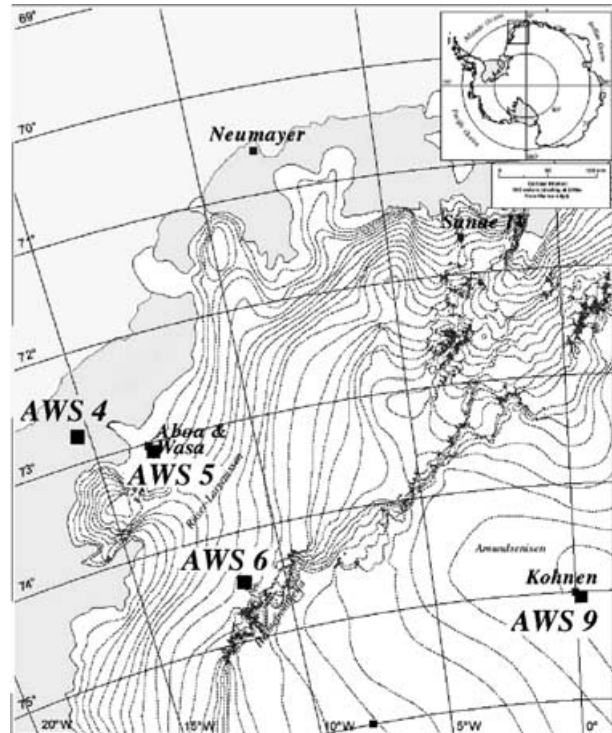


Fig. 1. Map of Western Dronning Maud Land, with the locations of four snow pits near the automatic weather stations. The locations of pit KOH 1 and pit KOH 2 (in the vicinity of Kohnen Station) are not shown as a result of the scale of this map.

profiles are compared with the observed isotopic variability in samples from snow pits in order to understand the controls on the observed isotope variability. The temperature during accumulation and the variability of precipitation throughout the year are evaluated in Section 5. The implications for the $\delta^{18}\text{O}$ - T relationship is discussed in Section 6. Section 7 summarizes the results.

2. Isotope records

The snow pits from which we collected samples in the austral summer of 2001–2002 are located near four AWSs along a transect connecting the coastal ice shelf (AWS 4) with the high Antarctic plateau (AWS 9) (Fig. 1). The escarpment region (AWS 5 and 6) forms the transition between these two areas. The AWSs are all equipped with SHRs, which monitor surface height. Table 1 lists the topographic and meteorological characteristics of these four sites.

We collected samples of snow that accumulated while the AWSs were operational (Table 2). To avoid errors due to the variability of spatial accumulation (e.g. sastrugi), the ideal snow sampling location would be right underneath the SHR, which would facilitate estimation of the deposition time of the snow layers. This was done at AWSs 6 and 9. However, since the stations periodically need rebuilding to prevent them from being

Table 1. AWS topographic and climate characteristics, 1998–2001^a

	AWS 4	AWS 5	AWS 6	AWS 9
Start of observation	22 Dec 1997	3 Feb 1998	15 Jan 1998	1 Jan 1998
End of observation	21 Dec 2001	2 Feb 2001	14 Jan 2002	31 Dec 2001
Location	72°45.2'S, 15°29.9'W	73°06.3'S, 13°09.9'W	74°28.9'S, 11°31.0'W	75°00.2' S, 0°00.4'E
Elevation (m a.s.l.) ^b	34	363	1160	2892
Surface slope (m km ⁻¹)	0.1	13.5	15.0	1.3
SSMB ^c (kg m ⁻² a ⁻¹)	393	179	267	74
Snow density (kg m ⁻³)	406	383	396	307
Temperature (K)	253.4	256.8	252.6	230.0
Relative humidity(%)	93	83	78	93
Specific humidity (g kg ⁻¹)	1.03	1.01	0.72	0.17
10 m wind speed (m s ⁻¹)	5.7	7.9	7.7	4.8

^aSource: Van den Broeke et al. (2004).

^ba.s.l., above sea level.

^cSSMB, specific surface mass balance.

Table 2. Characteristics of samples taken from snow pits in the field season 2001–2002

	AWS 4	AWS 5	AWS 6	AWS 9	KOH 1	KOH 2
Location	15 m from AWS 4	2 m from AWS 5	Under SHR	Under SHR	100 m NW of AWS 9	1 km N of Kohlen
Sampling date	25 Dec 2001	17 Dec 2001	14 Jan 2002	17 Jan 2002	13 Jan 2002	25 Jan 2002
Depth of the pit (cm)	450	200	300	91.5	120	120
δ Sampling interval (cm)	2.0	2.0	2.0	1.5	1.5	1.0
ρ Sampling interval (cm)	5.0	5.0	5.0	2.5	2.5	2.5

covered by snow, the surface around an AWS can become disturbed at the rebuilding horizon. For this reason, the snow pits at AWSs 4 and 5 were dug at a safe distance from the stations. Pit AWS 9 is located ~2 km west of Kohlen Station; radar reflectors were placed directly downwind from the AWS, which caused a disturbance in the wind field. Surface characteristics at this site showed a possible higher contribution of windblown snow to the local accumulation relative to the surroundings. Near Kohlen Station, pit KOH, 1 near a temporary satellite station, and pit KOH 2 were dug and sampled at a resolution of 1.5 cm and 1.0 cm respectively. The other pits were sampled at a resolution of 1.5 or 2.0 cm (Table 2). As pit KOH 2 was situated 2 km to the north of Kohlen Station, the accumulation at this site was not disturbed by the presence of the radar reflectors or other obstacles.

We carried out snow density measurements within 50 cm of the snow sampling profile, at a vertical resolution between 2.5 and 5.0 cm (Table 2). The snow samples taken for isotope analysis were kept frozen during transport to avoid isotopic fractionation after sampling.

The $\delta^{18}\text{O}$ measurements were carried out at the Centre for Isotope Research in Groningen, The Netherlands, on a SIRA 10 isotope ratio mass spectrometer with an adjacent $\text{CO}_2\text{--H}_2\text{O}$ equilibration system. The resulting accuracy of the measurements is 0.10 ‰.

Figure 2 shows the results of the $\delta^{18}\text{O}$ measurements. Clearly, the isotope records cover more than the operational period of the AWSs (1998–2001), since for all AWS locations at least four summer maxima can be distinguished in the isotope records. The timescale plotted along the horizontal axis was established by starting a new year at each summer maximum. The SHR record was used to distinguish between seasonal and subseasonal isotopic maxima. The difference between isotope profiles from a high-accumulation area (AWS 4: ~393 mm w.e. yr⁻¹; w.e. = water equivalent) and a low-accumulation area (AWS 9: ~74 mm w.e. yr⁻¹) is apparent: in the isotope profile from AWS 4, much more intraseasonal detail has been preserved compared with the more sinusoidal records from around Kohlen Station (AWS 9, KOH 1 and KOH 2). Note that the horizontal scale of Fig. 2 is different for each pit, indicating the variation in thickness of the seasonal layers (see Section 5). Note also that the Kohlen Station pits tend to show sharp, narrow summer maxima and less pronounced, but more extended, winter minima.

3. Reconstruction of the seasonal isotopic variability

To be able to compare the isotopic composition of snow with the meteorological conditions prevailing during deposition on

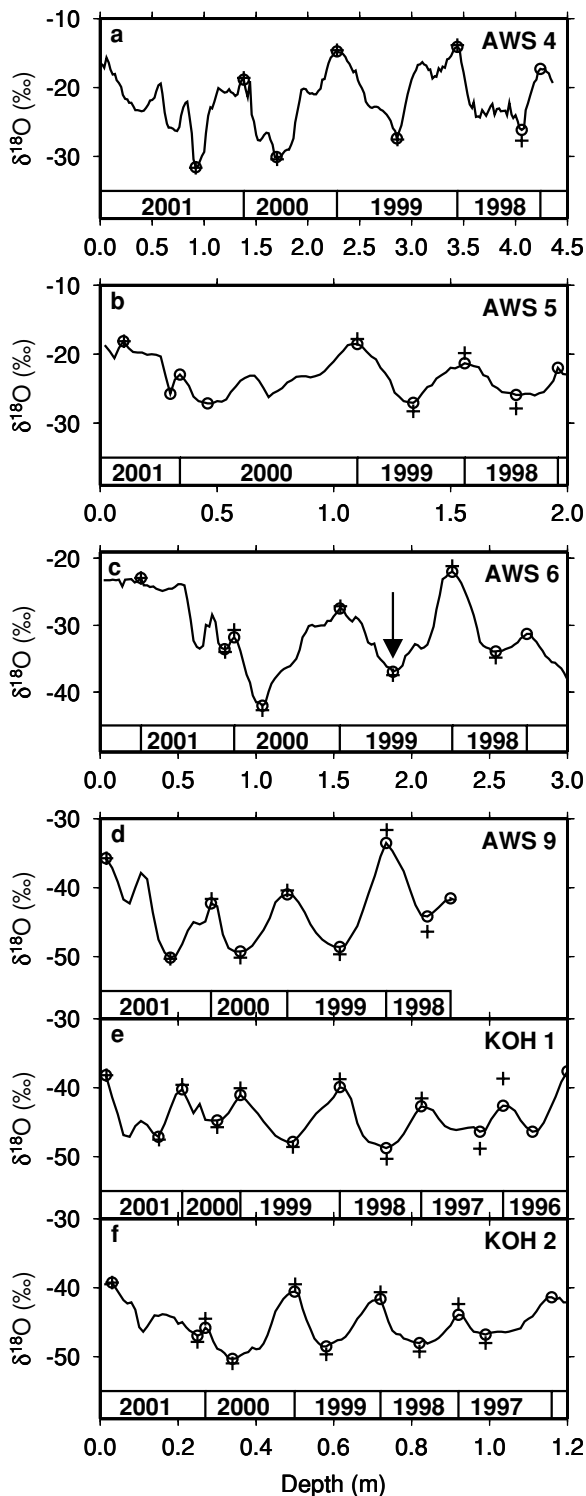


Fig 2. The isotope records from the snow pits at AWS 4, AWS 5, AWS 6, AWS 9, KOH 1 and KOH 2. The data are plotted at sampling resolution, no filtering has been applied. The seasonal extreme values of each year are indicated by circles. The plus signs show the back-diffused seasonal extreme values. A time indicator is shown above the x-axis, with a new year starting at each summer maximum.

an event base, the accumulation should meet two conditions. Firstly, to separate events in the isotope record, the accumulation per event should be greater than the sample resolution. Due to the low accumulation on the Antarctic plateau, it is probable that this condition is not always met at sites like AWS 9. Secondly, to allow us to neglect the influence of isotopic diffusion in the firn, low temperatures and high accumulation rates are optimal. Unfortunately, this combination is unlikely. Accumulation is high at the coastal ice shelf, but the temperatures are high as well, which enhances isotope diffusion. On the Antarctic plateau, temperatures are lower, but due to the much thinner seasonal snow layers diffusion will have a large influence as well, and affect longer timescales in the snow.

The shape of the isotopic records (Fig. 2) indicates that the seasonal amplitudes decrease with depth. Therefore we suspect that diffusion cannot be neglected in the study area, even though the time of sampling after deposition of the snow is relatively short (<4 yr). Since the focus of this study is on seasonal variability, the original seasonal isotope signal should be reconstructed; this can be done by using a back-diffusion model.

Molecular mixing in air in the pores of the ice matrix dominates isotope diffusion in firn. Johnsen (1977) first described the physics of this process; this description was later improved by Whillans and Grootes (1985), Cuffey and Steig (1998) and Johnsen et al. (2000). The back-diffusion method we used is based on the diffusion theory of Johnsen et al. (2000), in which two earlier diffusion equations of Johnsen (1977) and Whillans and Grootes (1985) are combined successfully. Their model describes the smoothing of isotope profiles over time; this smoothing appears to be strongly dependent on temperature and firn density. Density and temperature gradients in the firn would theoretically also influence the magnitude of diffusion, but this effect is so small that it can be neglected (Whillans and Grootes, 1985). Following Johnsen et al. (2000), the isotopic composition δ of (not deforming) firn at a depth z changes over time t according to:

$$\frac{\partial \delta}{\partial t} = D(z, t) \frac{\partial^2 \delta}{\partial z^2}. \quad (1)$$

The diffusivity D depends for each isotopic species on the temperature T and density ρ of the firn. For the diffusion of $\delta^{18}\text{O}$, Johnsen et al. (2000) defined D as follows:

$$D(z, t) = \frac{m e_{si}(T) \omega_{a18}(T, P)}{RT \alpha_{18} \tau} \left(\frac{1}{\rho} - \frac{1}{\rho_{ice}} \right). \quad (2)$$

Here, m is the molar weight of water, e_{si} is the saturation vapour pressure over ice, ω_{a18} is the diffusivity of the heavy isotope (i.e. H_2^{18}O) in the open air, P is the ambient air pressure, R is the universal gas constant, α_{18} is the ice–vapour equilibrium fractionation factor for ^{18}O and τ is the tortuosity. For all parameters in this equation we use expressions as suggested by Johnsen et al. (2000).

Equation (1) can be used to model the diffusion of the isotope signal over time. However, a back-diffusion model is needed

to reconstruct the undiffused signal from the isotope record. Reversing the diffusion process numerically leads to unstable results because the input isotope record often shows high-frequency variations that quickly blow up to unrealistic values. Even in originally smooth isotope records, artificial intraseasonal variations develop during back-diffusion modelling. Filtering of the original data is a solution to these problems (e.g. Johnsen, 1977; Cuffey and Steig, 1998; Bolzan and Pohjola, 2000), but has the drawback that it has the same effect as forward-diffusion: it leads to a small but unknown underestimation of the back-diffused amplitudes. Since our main objective was the reconstruction of the original seasonal amplitudes rather than subseasonal fluctuations we preferred not to filter the data, but to use a simpler numerical approach described by Bolzan and Pohjola (2000).

This approach only reconstructs the seasonal amplitude based on the extreme values of the isotope record (circles in Fig. 2) and calculates the back-diffused values from this reduced data set. The second derivative needed in eq. (1) is estimated by assuming that the isotopic variation around an extreme value is sinusoidal. At closely spaced seasonal extremes, this assumption may not hold, but this method generally leads to realistic reconstructions (Bolzan and Pohjola, 2000). The second derivative in eq. (1) is then approximated by:

$$\frac{\partial^2 \delta}{\partial z^2} = \pm \frac{1}{2} \pi^2 \left(\frac{A_i}{\lambda_i^2} + \frac{A_{i+1}}{\lambda_{i+1}^2} \right) \quad (3)$$

where $A_{i(+1)}$ is the isotopic amplitude above (below) an extreme value i and $\lambda_{i(+1)}$ is the seasonal layer thickness above (below) an extreme value i . The plus (minus) sign indicates an isotopic trough (crest). Using this method, we solved the diffusion equation by keeping the upper boundary value fixed, which means that the surface snow is not altered by diffusion. We set the value of the second derivative of the lower boundary equal to the neighbouring extremum (but with the opposite sign), which may introduce a small error, but we omit the last extremum in each pit in the analysis discussed in Section 6.

We let the calculation start at the moment of sampling, and step backward in time, in steps of 1 d. Since T and ρ are the key parameters that control the diffusivity coefficient, it is important to use the correct values. We used modelled daily subsurface temperatures from an energy balance model applied to the AWS data (Van den Broeke et al., in press). For the density we used a fitted function through our density measurements for each snow pit, and assumed that this density distribution is constant over time.

This back-diffusion method considers the firm as a closed system; eventual enhanced diffusion due to wind pumping (Neumann and Waddington, 2004) is neglected, and the influence of isotopic fractionation associated with snow metamorphism (Friedman et al., 1991) is not taken into account. These assumptions will probably lead to a small underestimation of the back-diffusion in the upper part of the firm.

Table 3. Summary of results of the back-diffusion model

	Mean amplitude measured record (‰)	Mean amplitude back-diffused record (‰)	Change (%)
AWS 4	6.6	7.0	5
AWS 5	3.1	3.7	19
AWS 6	5.4	5.9	9
AWS 9	5.0	5.9	19
Pit KOH 1	3.6	4.4	22
Pit KOH 2	3.5	4.2	22

In Fig. 2, the plus signs indicate the back-diffused seasonal extremes. Although the differences between measured and modelled extremes do not appear to be very large, the diffusion cannot be neglected: Table 3 lists the average seasonal amplitudes of both the measured and the back-diffused records, as well as the relative increase in amplitude. These data show that the seasonal extremes at AWS 5 and at the Antarctic plateau (AWS 9, KOH 1 and KOH 2) have experienced the greatest relative change ($\sim 20\%$), which implies that these isotope profiles are most vulnerable to diffusion effects. Relative increases of the seasonal isotope amplitude directly result in equal relative increases of the seasonal $\delta^{18}\text{O}-T$ slope.

Although the model yields consistent results both in forward and backward modes, the accuracy of the back-diffused seasonal extremes is difficult to assess since the results cannot be validated. However, the calculations provide the most plausible estimation of the influence of diffusion on the annual isotope cycles. Sampling of snow pits over successive years would provide valuable data for testing the robustness of the back-diffusion method.

In general, the model seems to have generated realistic values, with one exception: the seasonal extreme values at AWS 5 from the winter of 2000 to the winter of 2001 (not shown in Fig. 2). The thin seasonal layer at this location did not allow the assumption of a sinusoidal shape of the δ curve near the extreme values. This resulted in an erroneous reconstruction, due to an overestimation of the second derivative in eq. (3).

According to our results, diffusion has an almost negligible effect on the seasonal amplitude at AWS 4. However, the observed subseasonal variation in the record of AWS 4 has not been reconstructed, and it should be stressed that the method used here is not applicable to reconstruct subseasonal variability. Therefore, the original subseasonal variation may have been larger than the measured variation.

4. Accumulation record

The local meteorology and accumulation have been monitored with four similar AWSs (see Reijmer and Van den Broeke, 2003, for a detailed description). Table 1 gives a summary of the topographic and climatic characteristics of the AWS sites.

For this study, we mainly used the results of the SHRs (Campbell SR50), which measured (the change in) surface height. Every 2 h the instruments measured a time lag between a downward sonic signal and the first received reflected upward sonic signal. Since temperature influences the speed of sound, a temperature correction was applied. The SHR data were filtered with a moving average over a day, after which the record was subdivided into 12-h intervals.

The SHR records of the change in surface height at the four AWSs are plotted in Fig. 3a. All four records are characterized by

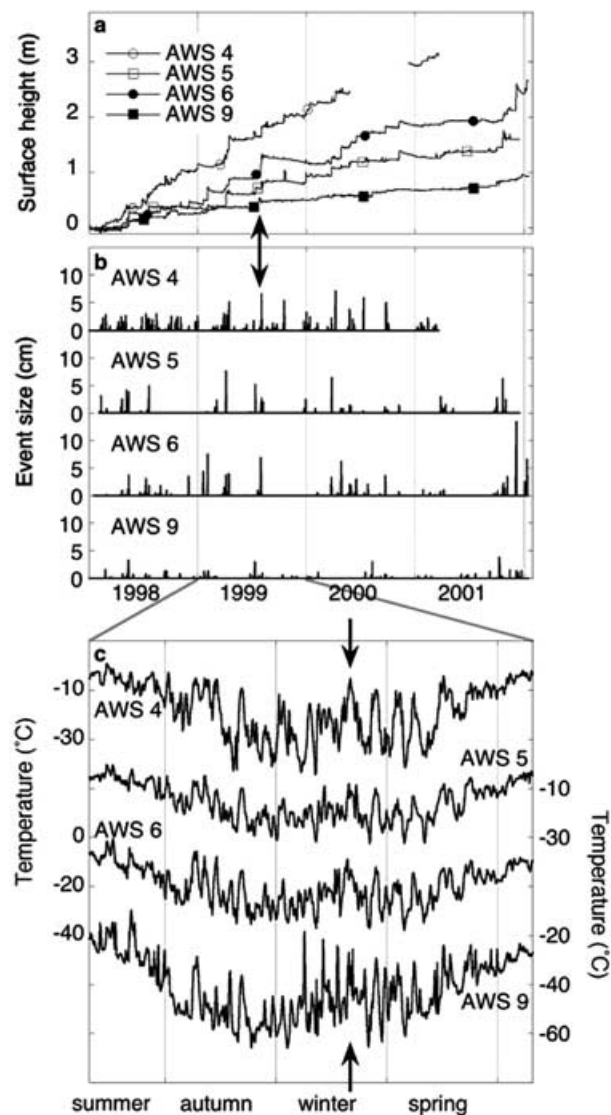


Fig 3. Surface height (a) and identified accumulation events (b) from the AWSs over the period 1998–2001. Due to a malfunctioning SHR, the accumulation history of AWS 4 could only be established until early 2001, with a data gap in winter 2000. The temperature records (daily means) of 1999 are shown in (c). The arrows point to an accumulation event at all four sites in early August 1999.

discontinuous, sharp increases of the surface height, followed by longer periods of slowly decreasing or constant surface height. The sudden increases in the surface height are caused by snow deposition: a combination of snowfall and a net deposition of drifting snow. The SHR record does not distinguish between the two types of accumulation, but since most of the accumulation events occur simultaneously with events at at least one other AWS, accumulation appears to be predominantly the result of snowfall. During the periods without accumulation, the surface slowly subsides as a result of settling of the snow and sublimation. Sharper decreases in the surface height are caused by net erosion due to snowdrift.

Note that not all snowfall events have been preserved in the snow pack, since sublimation and snowdrift may have partly removed the accumulated snow. Figure 4 displays a close-up of the SHR record. The surface of the snow that accumulated on 26 May 2000 slowly dropped (due to settling, sublimation or wind erosion), until a new accumulation event covered this snow on 29 May 2000, after which the cycle was repeated. An accumulation date was attributed to a snow layer as soon as new accumulation permanently buried the previous layer (Fig. 4). The top level of this previous layer is then defined as the base level of the new layer. Due to settling of underlying snow, the distance between a certain snow layer and the SHR increases slowly with time. A depth correction using the density measurements was carried out on the SHR data to facilitate comparison with the isotope records. Unfortunately, not all isotope records were sampled at the exact same position as the SHR records (Table 2), which makes such a comparison not always straightforward since local

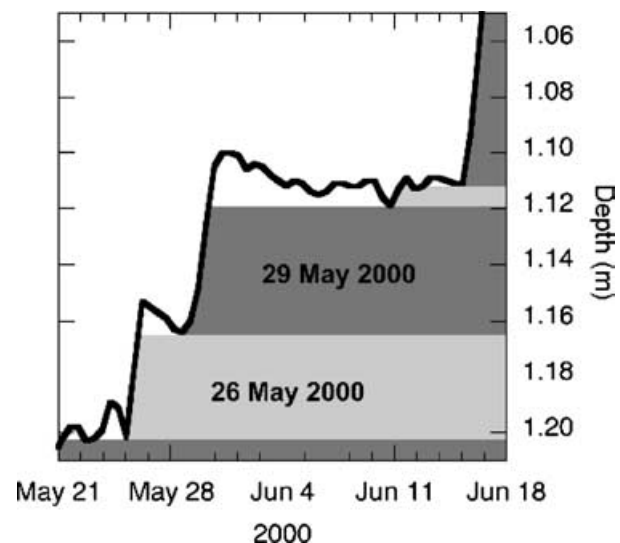


Fig 4. Example of the attribution of an accumulation date to a snow layer. The thick line indicates the SHR data for AWS 6. As soon as the surface height data show a new accumulation event (e.g. at 12:00 h on 29 May 2000), an accumulation date is given to the underlying snow.

variability of accumulation can be large (e.g. Richardson et al., 1997; Frezzotti et al., 2002; King et al., 2004).

All preserved accumulation events were identified from the record of the surface height change, as explained in Figure 4. Fig. 3b shows an overview of the timing and magnitude of these events. The monitoring period is too short to draw strong conclusions about seasonality. Nevertheless, for AWS 9 we observe a tendency towards increased accumulation in winter. This would explain the relatively broad winter minima in the isotope records compared with the narrow summer peaks.

The intermittent character of accumulation in this area is apparent: only a few large events account for the bulk of the total accumulation. Reijmer and Van den Broeke (2003) have described the size distribution of accumulation events in more detail. The lack of accumulation over long periods of the year may result in an isotope record that is not representative of the mean annual temperature. This will be further investigated in the next section.

5. Temperature during accumulation

To investigate the temperature signal in the $\delta^{18}\text{O}$ records it is valuable to compare them with the temperature records from the AWSs (e.g. Shuman et al., 1995; Van Ommen and Morgan, 1997). However, as accumulation in DML is discontinuous and the $\delta^{18}\text{O}$ signal is determined by conditions during accumulation, a comparison with a continuous temperature record is not appropriate since this study is trying to reveal the local controls of the $\delta^{18}\text{O}$ - T relation. Therefore, we analyse the temperature records using the time-series of the accumulation events. As an example, Fig. 3c shows the daily temperatures of 1999 as measured by the AWSs. In winter especially, the temperature is highly variable; higher than average temperatures often coincide with accumulation in DML. This is in agreement with earlier findings for this area by Reijmer and Van den Broeke (2003) and can be explained by the synoptic conditions that are characteristic for accumulation in this region: a low-pressure area over the Weddell Sea and a high-pressure area over eastern DML enhance advection of warm and humid air. The Antarctic plateau then forces the air to rise, inducing orographic precipitation (Noone et al., 1999).

The arrows in Fig. 3 highlight an example of these typical accumulation conditions. During this period in the middle of the Antarctic winter (August 1999), accumulation occurred at all four sites. Figure 3c shows that in that period all four AWSs recorded daily mean temperatures that are comparable with summer conditions. The difference in temperature between snowfall events and average seasonal conditions causes a bias in the isotope record, since only snowfall conditions are preserved in the snow.

The temperature shown in Figures 3c is the 2-m temperature, $T_{2\text{m}}$, as measured by the AWSs. The isotopic composition of snow is not directly influenced by $T_{2\text{m}}$. Of greater importance is the temperature at the time and place of snow formation, i.e. the temperature during condensation, T_c . Therefore, we expect that

a comparison of the $\delta^{18}\text{O}$ records with T_c should lead to a better understanding of the $\delta^{18}\text{O}$ relationship.

We obtained T_c from a regional atmospheric climate model specially designed for the Antarctic region (RACMO2/ANT) (Reijmer et al., 2005). The European Centre for Medium Range Weather Forecasts (ECMWF) reanalysis data set ERA-40 drives RACMO2/ANT at its boundaries. RACMO2/ANT simulates the Antarctic climate at a horizontal resolution of ~ 55 km and with 40 vertical levels. RACMO2/ANT has proved to yield more realistic results for the Antarctic region than the ERA-40 data set itself (Reijmer et al., 2005). In the following we use vertical profiles from RACMO2/ANT at grid points close to the AWS locations in terms of location, elevation and slope.

Figure 5 depicts vertical profiles of temperature and condensed water (cloud water content, CWC) at the four AWS locations for two occasions. The solid lines represent the state of the atmosphere during warm conditions on 3 August 1999; the dashed lines show the clear-sky situation on 26 July 1999. These dates are representative examples of the state of the boundary layer during overcast and clear-sky conditions, respectively.

During clear-sky conditions (no CWC in Fig. 5), a temperature inversion develops in the atmospheric boundary layer, which explains the low surface temperatures. Cyclonic disturbances bring warmer and more humid air inland, which often leads to snowfall over the area. During these overcast conditions, no significant temperature inversion is present (Fig. 5) as the result of an increase in the surface net radiation budget. After the low-pressure system has passed, a stable stratification can redevelop and the surface temperatures drop to low winter values again. Large temperature changes in wintertime (as shown in Fig. 3c) are the result of switches between inversion and non-inversion conditions. The accompanying temperature differences at the surface can be greater than 30°C . For comparison, $T_{2\text{m}}$ as measured by the AWS is plotted in Fig. 5 as well, and shows that RACMO2/ANT is successful in simulating the near-surface layer. Only at AWS 4 is $T_{2\text{m}}$ slightly underestimated.

With respect to the observed isotopic variability in the snow pits, we are interested in T_c during snow formation. For the definition of T_c , the profiles of CWC are of critical importance. A zone with nearly constant temperature can be found at the level of maximum CWC. This level of maximum CWC is defined as the level of snow formation, and the temperature at this level is T_c . Since RACMO2/ANT is only forced at its boundaries, it is free to simulate the climate within its domain. Consequently, it is possible that cyclonic systems arrive a few days later or earlier above DML than calculated. Therefore, we applied a search window of 6 d around the observed accumulation day to find the right moment of maximum CWC that is comparable with the AWS data.

In comparison with the strong difference in $T_{2\text{m}}$ between clear-sky conditions and accumulation conditions, we also see a somewhat higher temperature above the atmospheric boundary layer during snowfall, though not as large as for $T_{2\text{m}}$.

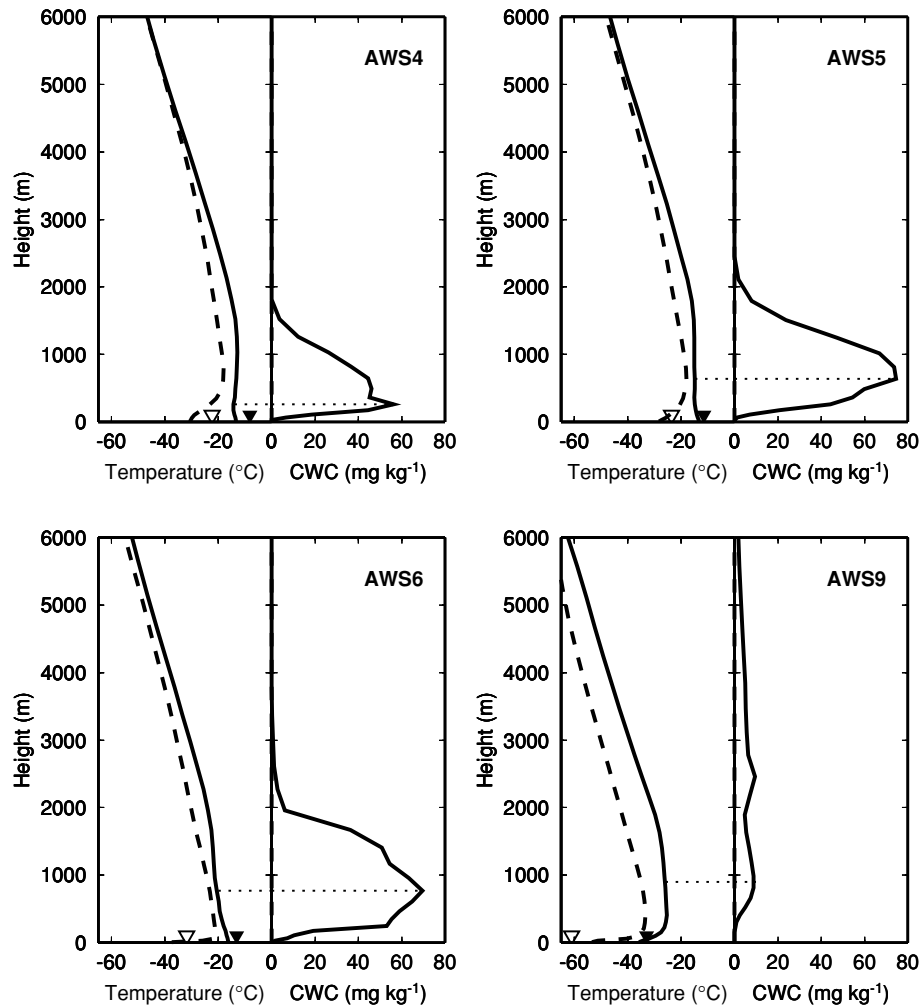


Fig 5. Vertical profiles of temperature (left) and cloud water content (CWC) (right) at the four sites. On 26 July (dashed lines), clear-sky conditions prevail over DML, which caused a temperature inversion in the atmospheric boundary layer. On 3 August (solid lines), warmer and more humid air brought snowfall to the area. For comparison, the 2-m temperatures as measured by the AWS are plotted as triangles. The levels of maximum CWC and accompanying T_c are indicated by the thin dotted lines.

To further investigate the link between the temperature history and the observed isotopic records, we retrieved T_{2m} (from the AWSs) and the T_c (from RACMO2/ANT) for all events that were greater than the SHR event resolution (1 cm). These temperatures are plotted in Fig. 6, and form synthetic temperature records at the resolution of sampling in the snow pits (T_{2m} as white dots and T_c as black dots). Due to the threshold of 1 cm, only relatively large accumulation events contribute to this temperature record. At AWS 9 in particular some of the events fell below this threshold, as a result of which no temperature is determined in some sample increments resulting in a discontinuous record (indicated by the white zones). The discontinuities in the record for AWS 4 are caused by inferior data from the SHR of this AWS.

The horizontal white lines in Fig. 6 represent the mean value of T_{2m} over the observed period for each site. For most precipitation events, T_{2m} is higher than this value, indicating that

a bias is introduced in the isotope records relative to annual means. Focusing on the preserved amplitude of both T_{2m} and T_c (Fig. 6; white and black dots, respectively), it appears that these amplitudes are smaller than the amplitude of the annual temperature cycles of T_{2m} in Fig. 3c. As snow formation occurs during non-inversion conditions or above a possible temperature deficit layer, the seasonal amplitude of the temperature preserved in the isotope record is smaller than the amplitude observed in the seasonal signal of T_{2m} .

The background colours in Fig. 6 indicate the season in which the snow accumulated. Only the data from AWS 4 represent all seasons during the observation period, i.e. no seasons are missing in the annual accumulation record. This is not surprising considering the high accumulation rates at this site on the coastal ice shelf. In the records from AWSs 5, 6 and 9, all lower accumulation sites, the seasons are often very poorly resolved, or

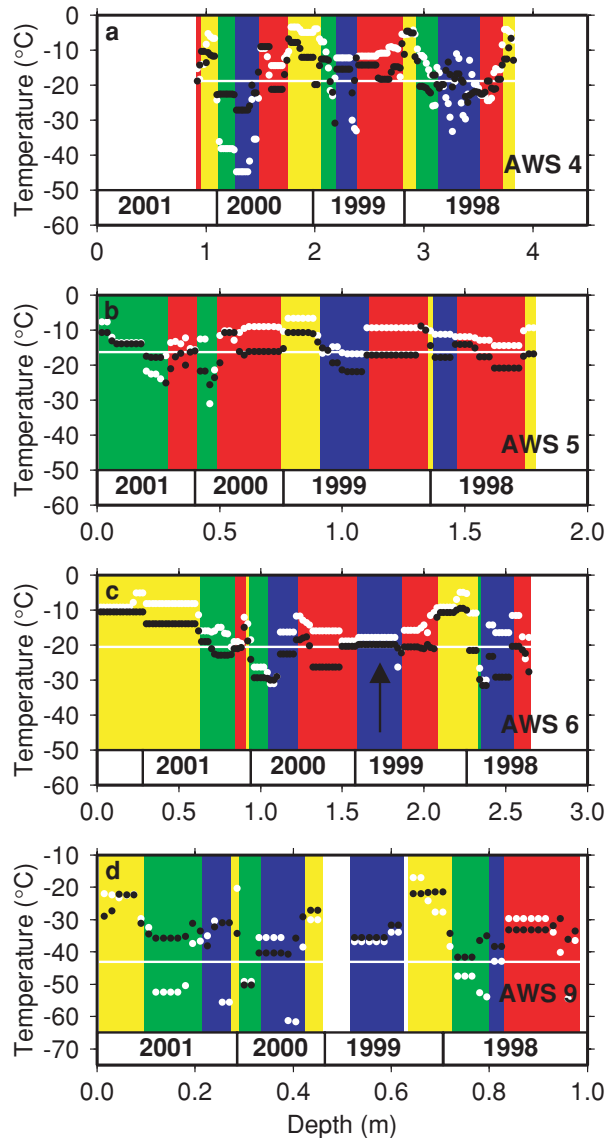


Fig. 6. T_{2m} (white dots) and T_c (black dots) during accumulation. The climatological value of T_{2m} is indicated by the horizontal white line. The background colours indicate the season of accumulation (green, spring (SON); yellow, summer (DJF); red, autumn (MAM); blue, winter (JJA)). A time indicator is displayed above the horizontal axis.

even lacking completely, e.g. the summer and winter of 2001 at AWS 5. This explains the lack of a pronounced seasonal cycle for 2001 in the isotope record of AWS 5 (Fig. 2b), and the problems arising with the reconstruction of these seasonal extreme values.

Nevertheless, for most years the isotope records exhibit a clear seasonal cycle (Fig. 2). However, the seasonal variations in the associated temperature records (Fig. 6) are much less pronounced. A good example that illustrates this is the shape of the temperature record for AWS 6 for 1999 (Fig. 6c) in comparison

with the isotope record of AWS 6 (Fig. 2c). The temperature during accumulation in autumn and winter 1999 (arrow in Fig. 6) remained on a constant level, close to the mean temperature over the total observed period. Nevertheless, in Fig. 2c the $\delta^{18}\text{O}$ record shows a clear winter minimum in the centre of the 1999 layer (arrow in Fig. 2), much lower than the $\delta^{18}\text{O}$ value of the preceding autumn. This qualitative comparison between the measured isotope records and the synthetic temperature records shows that T_c does not explain all variability in the isotope record. Certainly during winter precipitation, T_c often remains too high to explain the observed isotopic values in the moisture.

It should be stressed that due to the limited accuracy of the SHR, we only used temperatures prevailing during the larger accumulation events (>1 cm) for the construction of the temperature records in Fig. 6. Mainly for AWS 9, the exclusion of smaller events could potentially explain the lack of coherency between temperature and the $\delta^{18}\text{O}$ signal. However, we tested this potential error by also incorporating temperatures during accumulation events smaller than 1 cm. This barely changed the temperature records in Fig. 6, which supports our conclusion that local temperature variability cannot entirely explain the observed isotopic variability.

Besides T_c , it is the temperature difference over the distillation path that determines the isotopic composition of the moisture (e.g. Jouzel et al., 1997). An explanation for the observed values in the wintertime precipitation can be that the source region of this water vapour is situated more to the north, due to the increased extent of the sea ice in winter. For a better understanding of the observed isotopic variability, knowledge of the transport history is thus necessary.

6. Implications for the $\delta^{18}\text{O}-T$ relationship

This section quantifies the warm bias that is introduced in the isotope record and discusses its implications for the interpretation of the isotope records. Furthermore, the seasonal amplitudes of T_{2m} and T_c are compared with the observed seasonal isotope cycle by establishing seasonal $\delta^{18}\text{O}-T$ relationships. Figure 7 visualizes the temperature bias for the 4-yr period. Figure 7a shows a plot of the temperatures as measured by the AWSs during accumulation events, $T_{2m,\text{event}}$, against the average temperature of the month in which accumulation took place, $T_{2m,\text{month}}$. In general, $T_{2m,\text{event}}$ is higher than $T_{2m,\text{month}}$, and this effect becomes larger at lower temperatures. This indicates that the warm bias during accumulation is larger in winter. In addition, the scatter between $T_{2m,\text{month}}$ and $T_{2m,\text{event}}$ becomes larger with decreasing temperature, which means any relationship between $T_{2m,\text{month}}$ and $T_{2m,\text{event}}$ is not useful. This points out that with decreasing temperatures the individual accumulation events contain less information about average monthly conditions.

We calculated the mean deviation of $T_{2m,\text{event}}$ from $T_{2m,\text{month}}$ for each site, shown as the white bars in Fig. 7c. The magnitude of the introduced temperature bias is $\sim 4.5^\circ\text{C}$ for AWSs 4, 5 and

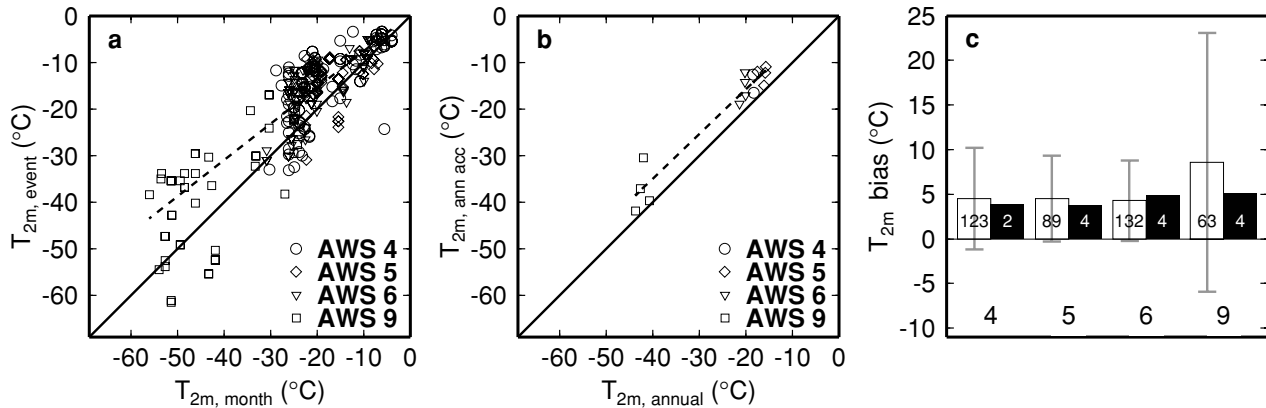


Fig 7. (a) Mean monthly values of T_{2m} versus $T_{2m,event}$ for all events. (b) Annual averaged values of T_{2m} versus mean annual values of $T_{2m,event}$. (c) The total temperature bias introduced in the accumulation records with its standard deviation. White bars indicate the average temperature bias of $T_{2m,event}$ from $T_{2m,month}$ (data from (a)). Black bars show the average temperature bias of $T_{2m,event}$ from $T_{2m,annual}$ (data from (b)). The number of points used for the averaging is indicated in the bars.

6. For AWS 9, this bias is much larger, $\sim 8.5^{\circ}\text{C}$. This large bias is related to the low accumulation rate at this site: the deviation from average conditions will be relatively large at a site with little accumulation. However, the large magnitude of the standard deviation of this bias (also shown in Fig. 7c) is of particular importance for the interpretation of the isotope records. This again points out that fluctuations in isotopic composition between individual accumulation events are not readily interpretable as local temperature fluctuations.

These results show that the isotopic composition of individual accumulation events does not contain consistent temperature information. The question that remains is: what is the shortest timescale over which the isotope records in this area contain significant temperature information? Since our data only cover 4 yr we can only test the effect of annual averaging, and not for longer timescales. This effect is depicted in Fig. 7b. All temperatures during accumulation are averaged over a year, $T_{2m,ann,acc}$, and plotted against the annual temperature of the site, $T_{2m,annual}$. In each of the observed years, $T_{2m,ann,acc}$ is higher than $T_{2m,annual}$. The large scatter as observed in Fig. 7a is no longer present. This results in an apparently better relationship between $T_{2m,annual}$ and $T_{2m,ann,acc}$. On a spatial scale this holds true, and we only see a spatially nearly constant offset of $T_{2m,ann,acc}$ with $T_{2m,annual}$. This offset is depicted as the black bars in Fig. 7c. We did not calculate the standard deviation as we only had a few data points. If the temperature bias per location were to be equally large for each year, a simple correction could be made for the interpretation of isotope records (using the dotted line in Fig. 7b). However, even after annual averaging, $T_{2m,ann,acc}$ shows large differences between the years (over 10°C for AWS 9), in contrast to $T_{2m,annual}$, which shows at most a difference of 2°C . Furthermore, the AWS 9 data reveal that the warmest year according to $T_{2m,ann,acc}$ is not the warmest year according to $T_{2m,annual}$ so, in other words, $T_{2m,ann,acc}$ and $T_{2m,annual}$ do not covary. The implication for the interpretation of isotope records in this area is that annual shifts

in $\delta^{18}\text{O}$ cannot be translated into changes in mean annual temperature, i.e. annual averaging of isotope data does not provide an accurate annual palaeothermometer for DML on these short timescales. However, we expect that an increase in the period of averaging to, for example to a decade, will lead to a more consistent relationship between temperature during accumulation and climate. This in turn would support the use of $\delta^{18}\text{O}$ as a climate proxy on these longer timescales.

This study also offers the possibility to address the relationship between annual mean values of T_{2m} and T_c during accumulation. This can be useful regarding the classical linear relation used in East Antarctica, linking inversion temperature and surface temperature (Jouzel and Merlivat, 1984). Although this transfer function is computed using spatial differences in the inversion strength, it is often used to translate changes in inversion strength over time. Although we only have a data for limited period, a comparison of time-series of annual mean values of T_{2m} and T_c weighted with accumulation (not shown) demonstrate that annual means of T_c during snowfall are not covariant with mean annual values of T_{2m} . This is in agreement with results of Van Lipzig et al. (2002), who pointed out that changes in the strength of the inversion layer can introduce large temperature biases on an interannual timescale.

Since the annual cycles in $\delta^{18}\text{O}$ and temperature are much larger than the interannual variation, a comparison of the annual isotopic cycle with the annual temperature cycle still seems valuable. To assess the relationship between the isotopic composition and the annual temperature cycle, we plotted the back-diffused seasonal extreme values of $\delta^{18}\text{O}$ against different associated temperatures. From these plots, we calculated the seasonal $\delta^{18}\text{O}$ - T slope (Table 4). Firstly, for Fig. 8a, we applied the method as described by Van Ommen and Morgan (1997), using the annual amplitude of monthly mean values of T_{2m} . All temperatures prevailing during the warmest and coldest months of the year have been used in this method, including non-accumulation days. The

Table 4. Characteristics of the $\delta^{18}\text{O}$ relationships at the different snow pit sites

	$T_{2\text{m,month}}$		$T_{2\text{m,event}}$		$T_{c,\text{acc}}$	
	Slope (‰ K ⁻¹)	<i>R</i>	Slope (‰ K ⁻¹)	<i>R</i>	Slope (‰ K ⁻¹)	<i>R</i>
AWS 4	0.55	0.97	0.42	0.97	0.57	0.96
AWS 5	0.60	0.98	1.16	0.98	0.83	0.96
AWS 6	0.67	0.90	0.65	0.94	0.77	0.88
AWS 9	0.37	0.93	0.27	0.81	0.49	0.84

The spatial slope from Oerter et al. (1999) has a value of 0.83 ‰ K⁻¹ (*R* = 0.99).

slopes from Fig. 8a are based on two areas of data points far apart in the graph, a winter minimum and a summer maximum. As a reference, the spatial $\delta^{18}\text{O}$ -*T* relationship for this area is also plotted (plus signs). This spatial slope is based on the mean isotopic composition of shallow firn cores and 10-m firn temperatures from coastal sites and sites on the Antarctic plateau in western DML (Oerter et al., 1999). The resulting slopes of the $\delta^{18}\text{O}$ -*T* relationships are all smaller than the spatial slope of this area (Table 4), which can be attributed to the fact that the winter temperatures used in this plot are the temperatures of the coldest month of each year. This is in line with findings of Van Ommen and Morgan (1997), for example.

We then used $T_{2\text{m,event}}$ during accumulation as well as T_c during accumulation (Figs 8b and c, respectively); if T_c is used, the $\delta^{18}\text{O}$ -*T* slopes become steeper, and more in line with the spatial slope, since condensation temperatures during accumulation are much higher than $T_{2\text{m,monthly}}$ in winter. Nevertheless, Fig. 8b shows that when $T_{2\text{m,event}}$ is used as a reference temperature, AWS 4 and 9 still have a low seasonal $\delta^{18}\text{O}$ -*T* slope. This is due to a persistent temperature inversion at these locations, since the slope of the regression line for AWS 4 and 9 is steeper

if T_c is used. At AWS 5 and 6, no strong temperature inversions occurred during large accumulation events.

Although it should be emphasized that the relationships derived in Fig. 8 are based on few data points, the seasonal $\delta^{18}\text{O}$ -*T* slopes (Fig. 8c) in general approach the spatial $\delta^{18}\text{O}$ -*T* relationship from Oerter et al. (1999). It is not unexpected that the ‘classical’ derived seasonal slopes (Fig. 8a) are all lower than the spatial slope, since the seasonal cycle will also influence temperature in the source area of the moisture. This will moderate the extra fractionation in winter, resulting in a smaller seasonal fluctuation in the $\delta^{18}\text{O}$ signal, and a low $\delta^{18}\text{O}$ -*T* slope. It is not likely that the spatial slope is influenced by this correlation of source and site temperature. Due to the use of T_c (Fig. 8c), the seasonal $\delta^{18}\text{O}$ -*T* slope increases, since the annual cycles of T_c are only small.

Although the newly derived seasonal slopes are comparable with the spatial slope, this result cannot be considered as support for the use of the spatial $\delta^{18}\text{O}$ -*T* relationship as a palaeothermometer on a seasonal scale, since as demonstrated above, the isotopic composition of individual events does not contain accurate information about monthly mean temperatures. Furthermore, selecting only temperatures during accumulation also leads to a weaker correlation coefficient *R* (Table 4) of the $\delta^{18}\text{O}$ -*T* relationship. The temperature at or above the accumulation site does not explain all of the observed isotopic variability. Besides, the established $\delta^{18}\text{O}$ -*T* relationships are sensitive to the inclusion or exclusion of one or more summer or winter maxima, indicating that the seasonal $\delta^{18}\text{O}$ variations in this area cannot reliably be interpreted as strictly variations in either the 2-m temperature or the temperature during snow formation.

7. Summary and conclusions

In this study, the relationship between isotopic composition of snow and temperature during snow formation has been assessed.

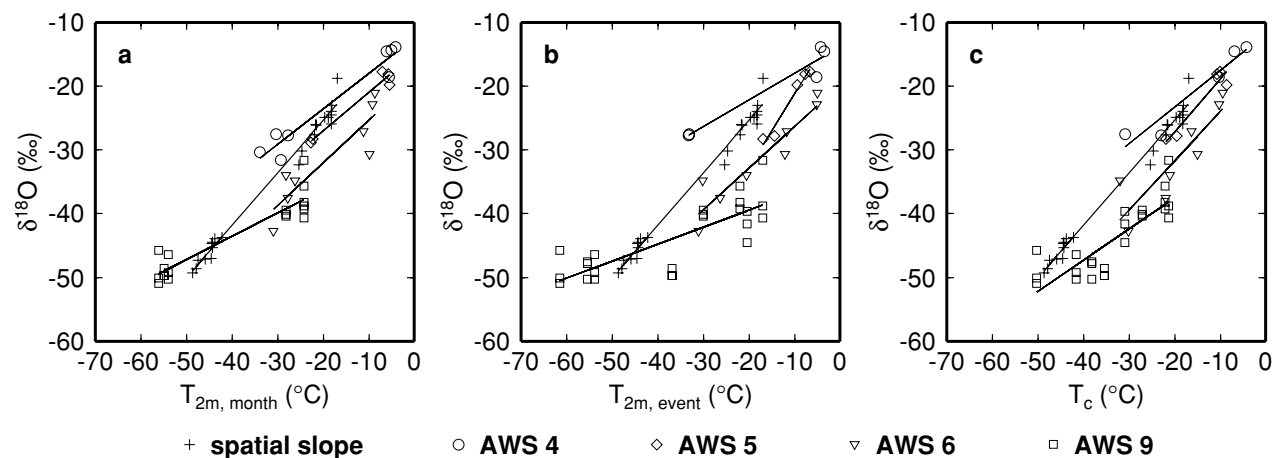


Fig. 8. $\delta^{18}\text{O}$ -*T* relationships, using (a) seasonal extreme values of $T_{2\text{m,month}}$, (b) $T_{2\text{m,event}}$, and (c) T_c . The spatial slope (plus signs) is plotted as a reference.

The seasonal extremes of isotopic composition were reconstructed by using a back-diffusion model. AWS data revealed that temperature is above average during accumulation. This effect is most pronounced in winter and at low-accumulation sites such as the Antarctic plateau. This is in line with earlier findings of, for example, Peel et al. (1988), Noone et al. (1999) and McMorrow et al. (2001). More important for the climatic interpretation of isotope records is the high interannual variability in the temperature during accumulation, compared with the interannual variability in annual mean temperature. These results show that isotope records in this area are a poor indicator of local temperature on timescales of days to several years. The number of years over which averaging should be performed to obtain an isotope record that better covaries with temperature cannot be determined from a limited data set such as we used here.

Van Lipzig et al. (2002) used the temperatures at the level where precipitation is formed to quantify the possible effects of the warm bias and the effects of seasonality in precipitation. In this paper, we have presented a comparison between observed seasonal isotopic variations and temperatures at the level of snow formation. This comparison indicates that temperatures during accumulation are not able to explain the observed isotopic variability. This in turn points out that the isotope signal is not just determined by the local temperature but is a more complex regional signal, influenced by, for instance, conditions along the transport path of the water vapour and in the source region.

With regard to seasonal variability, our results indicate that the slope of the seasonal $\delta^{18}\text{O}-T$ relationship depends to a large extent on which temperature is considered. The slope is lowest when the annual cycle of monthly average values of $T_{2\text{m}}$ is used (Fig. 8a). If cloud temperatures during accumulation are considered, the slopes are greater and more comparable to the spatial $\delta^{18}\text{O}-T$ relationship (Fig. 8c), but the correlation coefficients are lower. This again indicates that in contrast to the apparent firm $\delta^{18}\text{O}-T$ relationship on a spatial scale, the seasonal variability of the isotopic composition in this area cannot just be explained by changes in 2-m temperature or even by the temperature at the level of snow formation. This leads us to conclude that, on a timescale of seasons to several years, the direct interpretation of isotope shifts in terms of temperature change is not recommended for this area. To derive a better physical relationship between observed meteorological data and isotopic variability, a better understanding of the relative contribution of the different stages of depletion along the water vapour transport path is crucial (e.g. Helsen et al., in press). Such an approach will be followed in a forthcoming paper.

8. Acknowledgments

Words of gratitude go to Dan Zwartz for his work in and organization of the 2001/2002 field seasons of GOFISH. Furthermore, we thank the members of the FINNARP and SWEDARP

2001–2002 expeditions, Veijo Pohjola for his remarks on isotope diffusion and three reviewers for their valuable comments.

This work is a contribution to the European Project for Ice Coring in Antarctica (EPICA), a joint ESF (European Science Foundation)/EC scientific programme, funded by the European Commission and by national contributions from Belgium, Denmark, France, Germany, Italy, The Netherlands, Norway, Sweden, Switzerland and the United Kingdom. This is EPICA publication no. 122. Financial support was obtained from the Netherlands Organisation for Scientific Research (NWO) by a grant of the Netherlands Antarctic Programme.

References

- Arastarain, A., Jouzel, J. and Pourchet, M. 1986. Past Antarctic Peninsula climate (1850–1980) deduced from an ice core isotope record. *Climatic Change*, **8**, 69–89.
- Bolzan, J. and Pohjola, V. 2000. Reconstruction of the undiffused seasonal oxygen isotope signal in central Greenland ice cores. *J. Geophys. Res.*, **105**(C9), 22 095–22 106.
- Cuffey, K., Clow, G., Alley, R., Stuiver, M., Waddington, E. and Saltus, R. 1995. Large Arctic temperature change at the Wisconsin-Holocene glacial transition. *Science*, **270**, 455–458.
- Cuffey, K. and Steig, E. 1998. Isotopic diffusion on polar firn: implications for interpretation of seasonal climate parameters in ice-core records, with emphasis on central Greenland. *J. Glaciol.*, **6**(14), 273–284.
- Dansgaard, W. 1964. Stable isotopes in precipitation. *Tellus*, **16**, 436–468.
- EPICA Community Members 2004. Eight glacial cycles from an Antarctic ice core. *Nature* **429**, 623–628.
- Fisher, D. 1991. Remarks on the deuterium excess in precipitation in cold regions. *Tellus* **43B**, 401–407.
- Frezzotti, M., Gandolfi, S. and Urbini, S. 2002. Snow megadunes in Antarctica: sedimentary structure and genesis. *J. Geophys. Res.*, **107**(D18), 4344, doi:10.1029/2001JD000673.
- Friedman, I., Benson, C. and Cleason, J. 1991. Isotopic changes during snow metamorphism. In: *Stable Isotope Geochemistry: a Tribute to Samuel Epstein*, Geochemical Society Special Publication no. 3 (eds H. P. Taylor, R. O'Neill Jr and I. Kaplan). The Geochemical Society, St Louis, MO, 211–221.
- Graf, W., Oerter, H., Reinwarth, O., Stichler, W., Wilhelms, F., Miller, H. and Mulvaney, R. 2002. Stable-isotope records from Dronning Maud Land, Antarctica. *Ann. Glaciol.*, **35**, 195–201.
- GRIP Members 1993. Climate instability during the last interglacial period recorded in the GRIP ice core. *Nature*, **6**(14), 203–207.
- Helsen, M., Van de Wal, R., Van den Broeke, M., Kerstel, E., Masson-Delmotte, V., and co-authors. Modelling the isotopic composition of snow using backward trajectories: a particular accumulation event in Dronning Maud Land, Antarctica. *Ann. Glaciol.*, **39** (in press).
- Isaksson, E., van den Broeke, M., Winther, J.-G., Karlöf, L., Pinglot, J. and co-author 1999. Accumulation and proxy temperature variability in Dronning Maud Land, Antarctica, determined from shallow firn cores. *Ann. Glaciol.*, **29**, 17–22.
- Johnsen, S. 1977. Stable isotope homogenization of polar firn and ice. In: *Isotopes and Impurities in Snow and Ice*, IAHS Publication 118.

- International Association of Hydrological Sciences, Washington, DC, 210–219.
- Johnsen, S., Clausen, H., Cuffey, K., Hoffmann, G., Schwander, J. and co-author 2000. Diffusion of stable isotopes in polar firn and ice: the isotope effect in firn diffusion. In: *Physics of Ice Core Records*, (ed. T. Hondoh). Hokkaido University Press, Sapporo, 121–140.
- Johnsen, S., Dahl-Jensen, D., Dansgaard, W. and Gundestrup, N. 1995. Greenland palaeotemperatures derived from GRIP bore hole temperature and ice core isotope profiles. *Tellus* **47B**, 624–629.
- Jouzel, J., Alley, R., Cuffey, C., Dansgaard, W., Grootes, P. and co-authors 1997. Validity of the temperature reconstruction from water isotopes in ice cores. *J. Geophys. Res.* **102**(C12), 26 471–26 487.
- Jouzel, J. and Merlivat, L. 1984. Deuterium and oxygen 18 in precipitation: modeling of the isotopic effects during snow formation. *J. Geophys. Res.*, **89**(D7), 11 749–11 757.
- Jouzel, J., Vimeux, F., Caillon, N., Delaygue, G., Hoffmann, G. and co-authors 2003. Magnitude of isotope/temperature scaling for interpretation of central Antarctic ice cores. *J. Geophys. Res.* **108**(D12), 4361, doi:10.1029/2002JD002677.
- Karlöf, L., Winther, J.-G., Isaksson, E., Kohler, J., Pinglot, J. and co-authors 2000. A 1500 year record of accumulation at Amundsenisen western Dronning Maud Land, Antarctica, derived from electrical and radioactive measurements on a 120 m ice core. *J. Geophys. Res.* **105**(D10), 12 471–12 483.
- Kavanaugh, J. and Cuffey, K. 2003. Space and time variation of $\delta^{18}\text{O}$ and δd in Antarctic precipitation revised. *Global Biogeochem. Cycles*, **17**(1), 1017, doi:10.1029/2002GB001910.
- King, J., Andersen, P., Vaughan, D., Mann, G., Mobbs, S. and co-author 2004. Wind-borne redistribution of snow across an Antarctic ice rise. *J. Geophys. Res.* **109**(D11104), doi:10.1029/2003JD004361.
- Loewe, F. 1936. The Greenland ice cap as seen by a meteorologist. *Q. J. R. Meteorol. Soc.*, **62**, 359–377.
- Masson-Delmotte, V., Delmotte, M., Morgan, V., Etheridge, D., van Ommen, T. and co-authors 2003. Recent southern Indian Ocean climate variability inferred from a Law Dome ice core: new insights for the interpretation of coastal Antarctic isotopic records. *Clim. Dynam.*, **21**(2), 153–166.
- McMorrow, A., Curran, M., van Ommen, T., Morgan, V., Pook, M. and co-author 2001. Intercomparison of firn core and meteorological data. *Antarct. Sci.* **13**(3), 329–337.
- Merlivat, L. and Jouzel, J. 1979. Global climatic interpretation of the deuterium-oxygen 18 relationship for precipitation. *J. Geophys. Res.*, **84**(C8), 5029–5033.
- Neumann, T. and Waddington, E. 2004. Effects of firn ventilation on isotopic exchange. *J. Glaciol.* **6**(14), 183–194.
- Noone, D., Turner, J. and Mulvaney, R. 1999. Atmospheric signals and characteristics of accumulation on Dronning Maud Land, Antarctica. *J. Geophys. Res.* **104**(D16), 19 191–19 211.
- Oerter, H., Graf, W., Wilhelms, F., Minikin, A. and Miller, H. 1999. Accumulation studies on Amundsenisen, Dronning Maud Land, Antarctica, by means of tritium, dielectric profiling and stable-isotope measurements: first results from the 1995–96 and 1996–97 field seasons. *Ann. Glaciol.* **29**, 1–9.
- Peel, D., Mulvaney, R. and Davison, B. 1988. Stable-isotope/air-temperature relationships in ice cores from Dolleman Island and the Palmer Land plateau, Antarctic Peninsula. *Ann. Glaciol.* **10**, 130–136.
- Petit, J., Jouzel, J., Raynaud, D., Barkov, N., Barnola, J.-M. and co-authors 1999. Climate and atmospheric history of the past 420,000 years from the Vostok ice core, Antarctica. *Nature* **399**, 429–436.
- Reijmer, C. and Van den Broeke, M. 2003. Temporal and spatial variability of the surface mass balance in Dronning Maud Land, Antarctica, as derived from automatic weather stations. *J. Glaciol.* **49**(167), 512–520.
- Reijmer, C., Van Meijgaard, E. and Van den Broeke, M. 2005. Evaluation of temperature and wind over Antarctica in a Regional Atmospheric Climate Model using one year of automatic weather station data and upper air observations. *J. Geophys. Res.* **110**(D4), D04103, doi:10.1029/2004JD005234.
- Richardson, C., Aarholt, E., Hamran, S.-E., Holmlund, P. and Esaksson, E. 1997. Spatial distribution of snow in western Dronning Maud Land, East Antarctica, mapped by a ground-based snow radar. *J. Geophys. Res.* **102**(B9), 20 343–20 353.
- Robin, G. 1983. The climatic record from ice cores. In: *The Climatic Record in Polar Ice Sheets* (ed. G. Robin). Cambridge University Press, Cambridge, 180–195.
- Shuman, C., Alley, R., Anandakrishnan, S., White, J., Grootes, P. and co-author 1995. Temperature and accumulation at the Greenland Summit: comparison of high-resolution isotope profiles and satellite passive microwave brightness temperature trends. *J. Geophys. Res.* **100**(D5), 9165–9177.
- Van den Broeke, M., Reijmer, C. and Van de Wal, R. 2004. Surface radiation balance in Antarctica as measured with automatic weather stations. *J. Geophys. Res.* **109**, (D09103), doi:10.1029/2003JD004394.
- Van den Broeke, M., Van As, D., Reijmer, C. and Van de Wal, R. Seasonal cycles of Antarctic surface energy balance using automatic weather stations. *Ann. Glaciol.*, **41**, (in press).
- Van den Broeke, M., Van Lipzig, N. and Van Meijgaard, E. 2002. Momentum budget of the east Antarctic atmospheric boundary layer: results of a regional climate model. *J. Atmos. Sci.* **59**(21), 3117–3129.
- Van Lipzig, N., Van Meijgaard, E. and Oerlemans, J. 2002. The effect of temporal variations in the surface mass balance and temperature-inversion strength on the interpretation of ice-core signals. *J. Glaciol.* **48**(163), 611–621.
- Van Ommen, T. and Morgan, V. 1997. Calibrating the ice core paleothermometer using seasonality. *J. Geophys. Res.* **102**(D8), 9351–9357.
- Werner, M., Mikolajewicz, U., Heimann, M. and Hoffmann, G. 2000. Borehole versus isotope temperatures on Greenland: seasonality does matter. *Geophys. Res. Lett.* **27**(5), 723–726.
- Whillans, I. and Grootes, P. 1985. Isotopic diffusion on cold snow and firn. *J. Geophys. Res.* **90**(D2), 3910–3918.